

# Introduction of the linear contact model in the dynamic model of laminated structure dynamics: an experimental and numerical identification

MIHA PIRNAT<sup>1</sup>, GREGOR ČEPON<sup>2</sup>, MIHA BOLTEŽAR<sup>2</sup>

<sup>1</sup> KOLEKTOR ETRA d.o.o. ,

Šlandrova ulica 10, 1231 Ljubljana-Črnuče, SI-Slovenia

<sup>2</sup> University of Ljubljana, Faculty of Mechanical Engineering,  
Aškerčeva 6, 1000 Ljubljana, SI-Slovenia

---

## Postal address:

Miha Boltežar  
University of Ljubljana,  
Faculty of Mechanical Engineering,  
Aškerčeva 6, 1000 Ljubljana,  
SI-Slovenia

## Fax, Phone, E-mail:

Fax: + 386 1 2518-567  
Phone: + 386 1 4771-608  
E-mail: miha.boltezar@fs.uni-lj.si

## Cite as:

Miha Pirnat, Gregor Čepon, and Miha Boltežar

Introduction of the linear contact model in the dynamic model of laminated structure dynamics: an experimental and numerical identification. Mechanism and Machine Theory, accepted for publication.

DOI: 10.1016/J.MECHMACHTHEORY.2013.02.003

---

## Abstract

A numerical model of a laminated stack's dynamics applicable to general laminated structures was developed. A simple linear contact model facilitated the computational efficiency and in this way enabled the modelling of the stack's dynamics using a large number of laminas. The numerical model employs contact elements characterized by stiffness and damping parameters in a tangential contact direction and nonlinear contact stiffness in a normal contact direction. In order to identify the contact element parameters and to validate the developed numerical model of the laminated stack, several stack configurations were investigated using experimental modal analysis. The identified modal parameters were used in the optimization process to extract the contact element parameters. This made it possible to analyse the effects of the steel type, producer type, additional silicon layers and other treatments on the laminated stack's dynamics.

## Key words:

Laminated structure, electrical machine, contact model, dynamics

---

## 1. Introduction

A vast number of electrical devices, such as power transformers and electrical motors, contain laminated components made of sheets of electrical steel arranged in stacks and clamped together. Moreover, usually no adhesive is applied during the stacking. Under the influence of electromagnetic forces and magnetostriction these components exhibit undesirable mechanical vibrations and noise. The intensity of the vibrations depends on the dynamic properties of the structure and the magnitude of the excitation phenomena. By optimizing the design of the laminated structure the resonant frequencies can be avoided. However, for successful optimization it is necessary to develop a validated numerical model of laminated structures and to experimentally identify its general properties and dynamic behaviour.

Laminated structures are usually substantially more flexible than the equivalent homogeneous structures. They exhibit orthotropic behaviour and high levels of internal damping [1] due to interlaminar friction forces. The uneven surfaces of the laminations are responsible for the compressibility of the laminated cores, which was demonstrated in [2]. By optimizing the clamping pressure and other parameters that influence the friction damping, the vibration amplitudes can be substantially reduced [3-5]. In the case of a transformer core, the internal damping can also be greatly enhanced by the flexible bonding of laminations, which can reduce core vibrations by a factor between five and ten [6]. A number of studies [7-14] investigated the dynamic response of electrical machines with laminated components (e.g., stator). However, the finite-element models used in these studies did not include the effects of friction between the sheets. This could be a partial answer as to why the experimental results in the presented studies do not agree completely with the numerical results. Reasonably accurate results were achieved with 3D finite-element models using orthotropic material properties. The latter were proposed in order to account for a lower stiffness in the direction of sheet stacking in [10]. However, these simplified models were developed for a specific application and cannot be used for modelling general laminated structures. The proposed orthotropic material properties can lead to the occurrence of additional unrealistic mode shapes. Due to the limitations of the models presented in the literature we have developed a new, generally applicable numerical model of the laminated structure that incorporates interlaminar friction. The developed numerical model is based on experimental research that provided the dynamic properties of laminated stacks made of different types of electrical steel. The effects of the clamping force and the different stack configurations were also investigated and incorporated into the numerical model.

A simple linear friction contact law was used to model the interactions between the steel sheets, which allowed the use of implicit methods in the framework of linear structural dynamics. The stiffness and damping parameters of the contact model were identified using an optimization process that was based on a comparison between the experimentally and numerically obtained modal parameters of the laminated stacks. Once the identified contact parameters were used in a numerical model the numerically obtained modal shapes and the natural frequencies were in good agreement with the experimentally obtained data.

The article is organized as follows. The first section presents the stack configurations, the results of the experimental modal analysis and measurements of contact stiffness. In the second section the numerical model of a laminated stack is presented along with the model's assumptions and limitations. In the last section the optimization algorithm for the identification of the contact parameters is presented.

## 2. Experimental identification of the laminated stack's dynamic behaviour

In order to identify the dynamic properties of laminated stacks several stacks with different steel types, steel manufacturer and stack configuration were experimentally investigated. The stacks were composed of 240 steel sheets stacked in the  $z$ -direction, as shown in Fig. 1. The stack height, manufacturer identification number, steel type and stack configurations are given in Table 1.

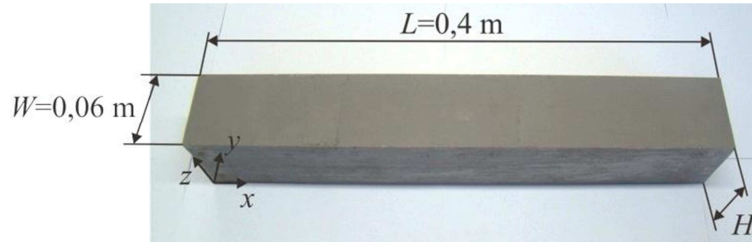
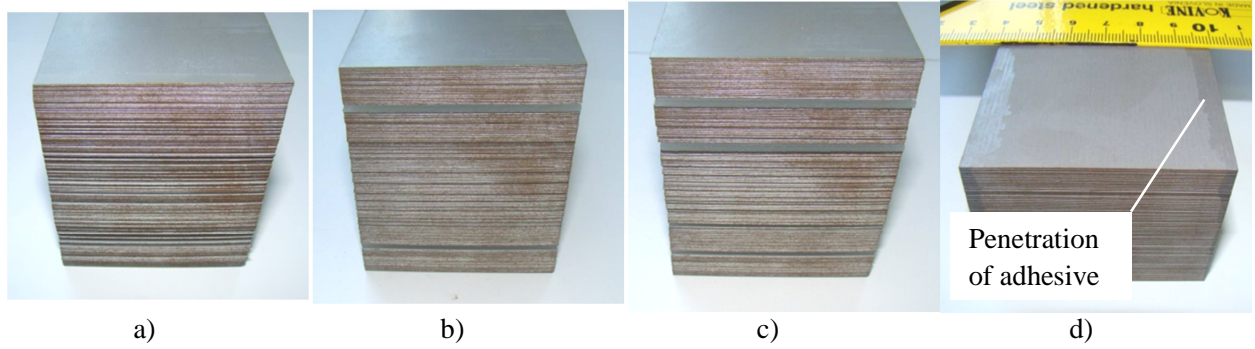


Figure 1: Dimensions of the laminated stack.

Table 1: Stack configurations used in the experimental analysis.

Stack number	Manufacturer identification number	Steel type	Treatment	Height [mm]
Stack 1	1	A	/	63.75
Stack 2	2	A	/	65
Stack 3	3	B	/	66.25
Stack 4	4	C	/	57.5
Stack 5	2	B	/	64.5
Stack 6	1	D	/	63.75
Stack 7	2	D	/	65
Stack 8	5	B	/	67.5
Stack 9	1	E	/	65.75
Stack 10	2	C	/	55.75
Stack 11	2	A	Lateral rolling direction of the steel sheets	65
Stack 12	2	A	Two 2-mm-thick silicon layers	65
Stack 13	2	A	Four 2-mm-thick silicon layers	65
Stack 14	2	B	Adhesive applied on the edges of laminations	64.5
Stack 15	4	C	Adhesive applied on the edges of laminations	57.5
Stack 16	5	B	Lubricated stack	67.5
Stack 17	3	B	Lubricated stack	66.25
Stack 18	1	A	Lubricated stack	63.75

Original stack configurations without any treatment, with two additional silicon layers, with four additional silicon layers and with adhesive applied at the stack edges are shown in Fig. 2. Due to the capillarity effect the adhesive penetrated into the space between laminas, as shown in Fig. 2d.



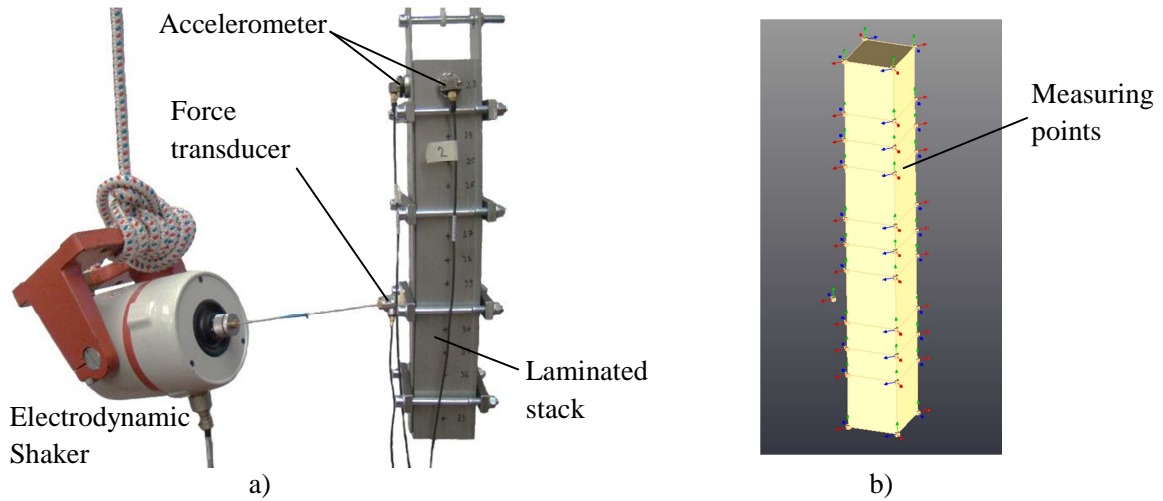
**Figure 2: Stack configurations: a) No treatment, b) Two additional silicon layers, c) Four additional silicon layers, d) The adhesive applied at the stack edges.**

For all the laminated stack configurations, first the modal parameters were experimentally obtained, which were then used to deduce the value of the contact parameters. Moreover, the experimental findings were crucial for the development of the numerical model.

Because the pressure distribution between the laminae is greatly influenced by the deformation of the stack in sheet-stacking direction [2] a measurement of the contact stiffness was also performed.

## 2.1 Identification of the modal parameters

The modal parameters were identified for all the stacks using an experimental modal analysis (EMA). The stacks were pressed together with four clamps that allowed the regulation of the clamping force. The system was excited with an electrodynamic shaker, as shown in Fig. 3a. A total of 45 measuring points were defined, one for the reference force transducer and 44 for the two roving accelerometers (Fig. 3b).



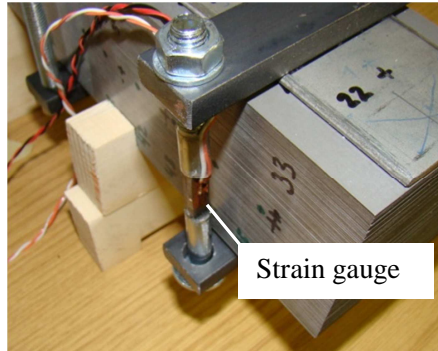
**Figure 3: Performing EMA: a) Experimental setup for EMA, b) Position of measuring points.**

The measurements were conducted for two values of lamina surface pressure, see Table 2. The chosen surface pressures correspond to typical values of the lamina surface pressures in the majority of electrical components.

**Table 2: Bolt tightening torque with corresponding lamina surface pressures.**

Bolt tightening torque	Lamina surface pressure
$M_1 = 1.5 \text{ Nm}$	160 kPa
$M_2 = 3 \text{ Nm}$	320 kPa

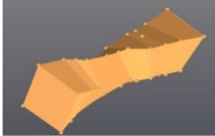
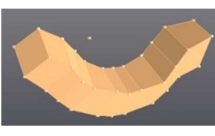

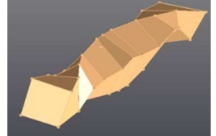
The relationship between the mean lamina surface pressure (clamping force) and the bolt tightening torque was identified by measuring the bolt stem deformation using strain gauges (Fig. 4).



**Figure 4: Strain gauges were used to identify relation between bolt axial force and tightening torque.**

In Table 3 the first four experimentally identified mode shapes are presented, which are identical for all the stacks. The mode shapes shown are the first torsional mode, the first bending mode, the second bending mode and the second torsional mode. The displacement of both bending modes takes place in the stacking direction of the steel sheets. The laminated stack has, in comparison to a homogeneous beam of equal dimensions, substantially lower natural frequencies and higher levels of internal damping.

**Table 3: First four experimentally identified mode shapes of a laminated stack.**

	1. Mode shape	2. Mode shape	3. Mode shape	4. Mode shape
Experimentally identified mode shape				

The natural frequencies and the modal damping ratios for some representative stacks are presented in Table 4. The values of the modal parameters differ regarding the steel type and the stack configuration. Furthermore, it can be observed that for the same steel type the values of the modal parameters depend on the steel manufacturer. This implies that the contact forces are mainly influenced by the surface roughness of the insulation layer that is covering the electrical steel sheets.

**Table 4: Modal parameters of the stacks.**

	Clamp bolts tightening torque	1. Mode shape		2. Mode shape		3. Mode shape		4. Mode shape	
		$f^a$ [Hz]	$\xi^b$ [/]	$f$ [Hz]	$\xi$ [/]	$f$ [Hz]	$\xi$ [/]	$f$ [Hz]	$\xi$ [/]
Stack 2	$M_1$	282	0.39	429	1.02	593	0.22	930	0.25
	$M_2$	280	0.14	474	1.2	665	1.79	979	0.37
Stack 3	$M_1$	272	1.18	298	1.55	531	3.05	932	1.23
	$M_2$	289	0.64	408	1.2	558	1.59	948	0.66

Stack 4	$M_1$	206	0.76	339	1.03	456	1.22	787	0.45
	$M_2$	231	0.37	371	0.79	499	1.4	855	0.38
Stack 8	$M_1$	279	0.75	411	1.57	551	3.1	868	1.32
	$M_2$	324	0.91	450	1.61	626	2.88	966	0.9
Stack 13	$M_1$	285	1.21	365	1.26	586	1.6	/ <sup>c</sup>	/ <sup>c</sup>
	$M_2$	246	0.91	386	0.17	626	1.4	/ <sup>c</sup>	/ <sup>c</sup>
Stack 15	$M_1$	285	0.82	348	3.19	484	3.71	782	0.2
	$M_2$	284	0.86	366	3.55	516	3.7	776	0.38
Stack 17	$M_1$	280	1.07	300	2.4	485	3.36	856	1.38
	$M_2$	291	0.9	404	2.05	591	3.91	996	1

<sup>a</sup> Natural frequency [Hz]

<sup>b</sup> Damping ratio [/]

<sup>c</sup> Could not be identified.

## 2.2 Identification of the contact stiffness

Frictional contact forces depend on the pressure distribution between the sheets of steel. It is shown in [2] that the contact stiffness has nonlinear characteristics due to the uneven surfaces of the steel sheets; moreover, it also depends on the stack thickness. Because the contact stiffness in the sheet stacking direction influences the pressure distribution between the laminas and in turn the frictional forces, it has to be experimentally identified.

For this purpose a sample laminated cube (Fig. 5) with the same height as the stacks under investigation was used. The experimentally obtained contact stiffness characteristic is shown in Fig. 6. Extensive deformation is observed at low values of the surface pressure due to the uneven surfaces that act as a spring. The measured contact stiffness will serve as an input contact parameter in the developed numerical model and will enable an accurate prediction of the contact pressure distribution between the laminas.

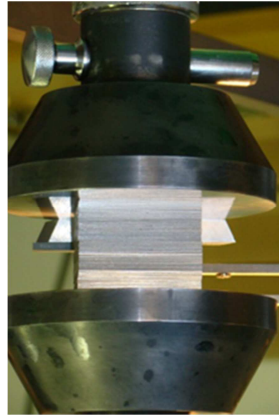


Figure 5: Contact stiffness measurement on a sample laminated cube.

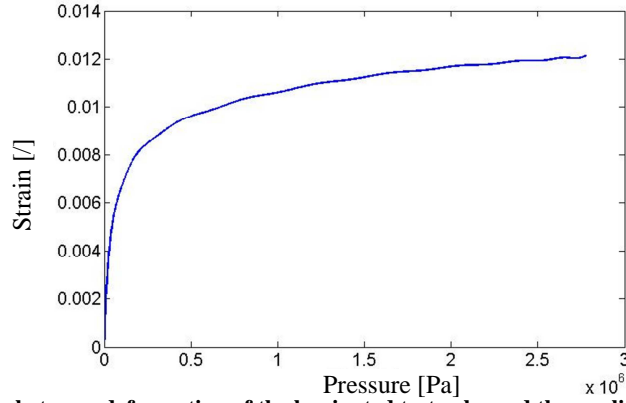


Figure 6: The relation between deformation of the laminated test cube and the applied surface pressure.

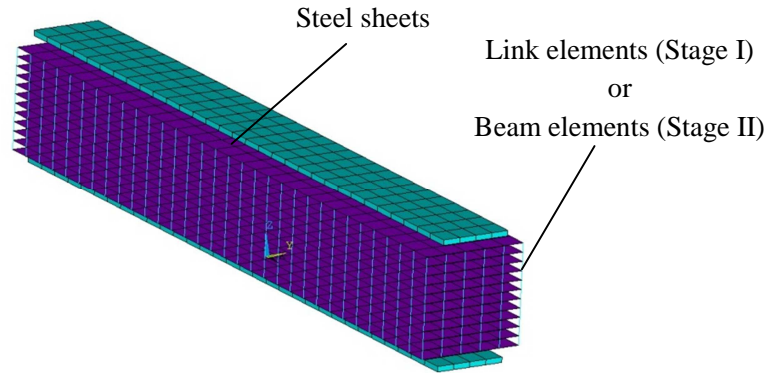
### 3. Numerical model of laminated stacks

The presented experimental results imply that the values of the modal parameters and thus the dynamic response of the stacks depend on the contact pressure distribution between the laminas, the surface roughness, the stack configuration, etc. Because these parameters influence the interlaminar frictional forces the developed numerical model will have to include the frictional forces between all the adjacent laminas. Thus each lamina has to be modelled separately using the frictional contact model.

The laminated stacks are modelled using Ansys shell181, link and beam4 elements, as shown in Fig. 7. The contact description between the adjacent laminas is based on a newly developed two-stage contact formulation. In the first stage the formulation proposes the use of nonlinear link elements for the modelling of the interlaminar pressure distribution. In the second stage a linear relation is assumed between the computed pressure distribution and the beam-element properties in order to model the effect of the friction forces and the sliding.

In the first stage the lamina surface pressure distribution is computed using static analyses based on a known clamping pressure. In order to correctly predict the distribution of the surface pressure the nonlinear contact stiffness has to be experimentally identified for a given height of the stack. For the modelling of the laminated stacks the measured relation shown in Fig. 6 was used for the nonlinear link stiffness in the normal contact direction, see Fig. 8. The cross-section of each link is defined according to the connected shell elements so that the combined surface of all the link cross-sections is equal to the lamina surface.

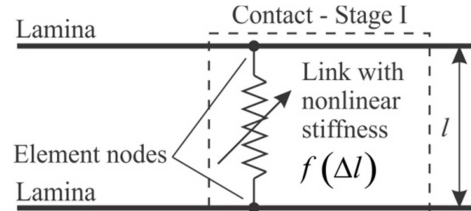
In the second stage the link elements are replaced with beam4 elements (Fig. 9) because of their shear capability. A linear relation is assumed between the computed surface pressure and the beam shear modulus where the slope is defined by the stiffness contact parameter  $G_f$  (Fig. 10a). Sliding in the contact is represented by a beam tangential deformation characterized via a beam shear modulus; therefore, no actual sliding occurs in the numerical model. The previously described technique is also applied for beam viscous damping characterization where the linear law slope is defined by the contact damping parameter  $d_f$  (Fig. 10b). The parameters  $G_f$  and  $d_f$  define the stiffness and the energy dissipation of the laminated stack, respectively. Additionally, their values clearly depend on the steel type, surface roughness, stack configuration, etc.



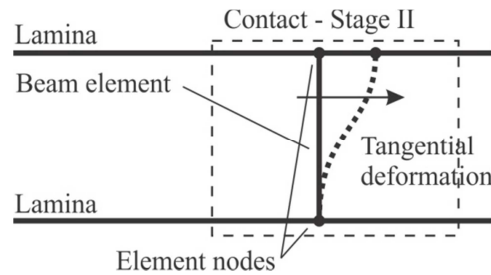
**Figure 7: Finite-element model of a laminated stack.**

In the normal contact direction a nonlinear stiffness is proposed in order to account for the initially extensive deformation due to the uneven surfaces. The nonlinear contact stiffness has to be experimentally identified for a given height of the stack, Fig. 8. This is crucial in order to correctly predict the distribution of the surface pressure.

The developed frictional model originates from models proposed in belt drive and tire dynamics. There the relative motion in the tangential direction is the result of the rubber-layer shear deflection and friction. Usually, this combined friction and shear deformation is modelled using a simple three-linear approximate friction law that permits some amount of sliding at low relative velocities [15]. This contact model is here modified as the frictional force depends on the relative displacement and velocity in the tangential direction, see Figures 8–10. Although the friction model is substantially simplified it gives a good prediction of the frictional forces between the laminae, especially when the relative displacement in the tangential contact direction is considered to be small.



**Figure 8: Modelling of the contact in stage I.**



**Figure 9: Modelling of the contact in stage II.**





**Figure 10: Friction law: a) Beam shear modulus in tangential contact direction, b) Beam viscous damping in tangential contact direction.**

### 3.1 Identification of the contact parametrs

The contact parameters  $G_f$  and  $d_f$  define the elastic and dissipative forces in the contact between adjacent laminas and thus the stiffness and energy dissipation of the whole laminated stack. As the values of the experimentally obtained modal parameters depend on the steel type, manufacturer, stack configuration, etc., it is expected that the contact parameters  $G_f$  and  $d_f$  will exhibit the same behaviour. For this reason the contact parameters will be identified for all the stack configurations presented in Table 1.

The identification of the contact parameters relies on the experimentally identified modal parameters presented in Table 4. The optimization function is defined as:

$$opt_G = \sqrt{\sum_{i=1}^4 (f_{exp,i} - f_{num,i}(G_f))^2}, \quad opt_d = \sqrt{\sum_{i=1}^4 (\xi_{exp,i} - \xi_{num,i}(d_f))^2}, \quad (1)$$

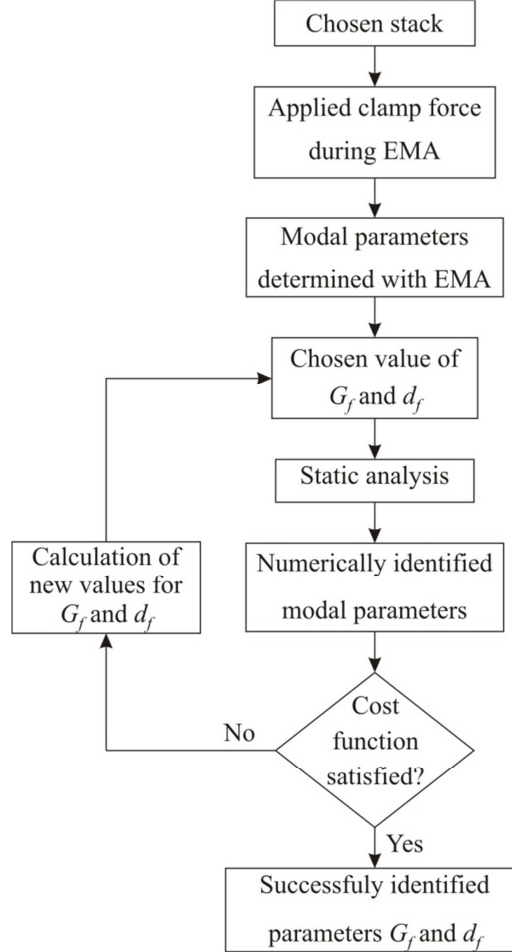
where  $f_{exp,i}$  is the  $i$ -th experimentally identified natural frequency and  $f_{num,i}$  is the numerically identified natural frequency. The  $\xi_{exp,i}$  and  $\xi_{num,i}$  are the  $i$ -th experimentally identified modal damping ratio and the  $i$ -th numerically identified modal damping ratio, respectively. The first four numerically identified modal shapes that were used in the optimization process are shown in Table 5. They are in good agreement with the experimentally obtained mode shapes (Table 3). The numerical model does not introduce any additional unrealistic mode shapes as this could be the case when the laminated structure is modelled as a solid with orthotropic material properties.

**Table 5: First four numerically identified mode shapes of a laminated stack.**

	1. Mode shape	2. Mode shape	3. Mode shape	4. Mode shape
Numerically identified mode shape				

The optimization algorithm is schematically presented in Fig. 11. First, for a given stack and selected clamping pressure the modal parameters are experimentally obtained. In the next step the guess values for the contact parameters  $G_f$  and  $d_f$  are determined. This is followed by a static analysis in order to deduce

the pressure distribution between the laminas. Finally, the modal parameters are numerically identified using the developed numerical model of the laminated stack. If the optimization functions  $opt_G$  and  $opt_d$  are within the prescribed tolerances, both contact parameters are deemed to be successfully identified, otherwise the procedure is repeated.



**Figure 11: Optimization algorithm for identification of the contact parameters.**

Using this optimization algorithm the contact parameters  $G_f$  and  $d_f$  were identified for all the stack configurations and surface pressures; however, the average contact parameters  $G_{f,avg}$  and  $d_{f,avg}$  between both surface pressures are used in the analysis of different treatments. The reason for this decision can be seen in Table 6. It is clear that the difference between identified contact stiffness parameters for different clamping pressures is small. Therefore, contact stiffness parameters could be assumed independent of the clamping pressure for a given stack configuration. Larger differences were noticed regarding the contact damping parameter, but this has only small effect on natural frequencies and mode shapes.

**Table 6: Identified contact parameters for representative stack configurations and different clamping pressures.**

Stack	$M_1$ (160 kPa)		$M_2$ (320 kPa)		Average	
	$G_f$	$d_f$	$G_f$	$d_f$	$G_{f,avg}$	$d_{f,avg}$
6	1147	7.4E-11	1012	4.60E-11	1079.50	6E-11

8	1625.3	1.45E-10	1487	7.70E-11	1556.15	1.11E-10
11	1049	1.16E-10	992	5.60E-11	1020.50	8.6E-11
12	1234	1.02E-10	1062	5.10E-11	1148.00	7.65E-11
14	1900.5	2.99E-10	1828	1.49E-10	1864.25	2.24E-10
16	1516	2.03E-10	1549	9.80E-11	1532.50	1.51E-10

The average contact parameters for the representative stacks are presented in Figures 12. They differ regarding the stack configuration, which implies that the frictional forces depend on the steel type, manufacturer and surface treatment of the steel sheets. In Fig. 13 the effect of additional silicon layers between the steel sheets is shown. These silicon layers were inserted into the laminated stack in order to reduce vibrations via an increased internal damping. However, adding silicon layers decreased the average contact damping parameters. This implies that friction between the adjacent laminas dissipates more energy than the inserted silicon layers.

The effect of the adhesive applied at the edges of the laminations is presented in Fig. 14. This has a minute influence on the value of the average contact stiffness parameter and it drastically increases the value of the average contact damping parameter. Thus, the application of the adhesive proves to be an efficient way to increase the internal damping. This is confirmed by the findings in [6]. The presence of a lubricant between the laminas increases the value of the average contact damping parameter by as much as 150%, but has practically no effect on the value of the average contact stiffness parameter (Fig. 15).

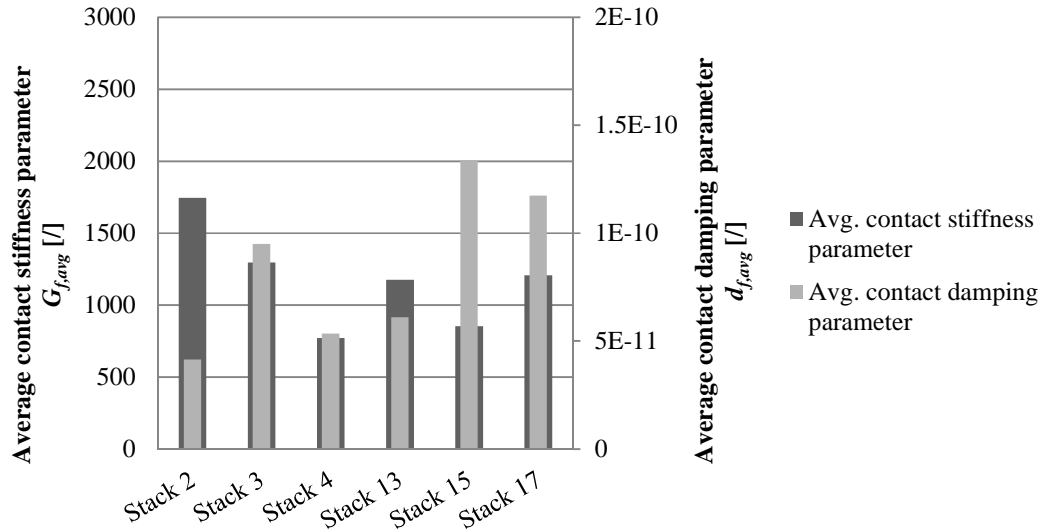


Figure 12: Identified average contact parameters  $G_{f,avg}$  and  $d_{f,avg}$  for the representative stacks.

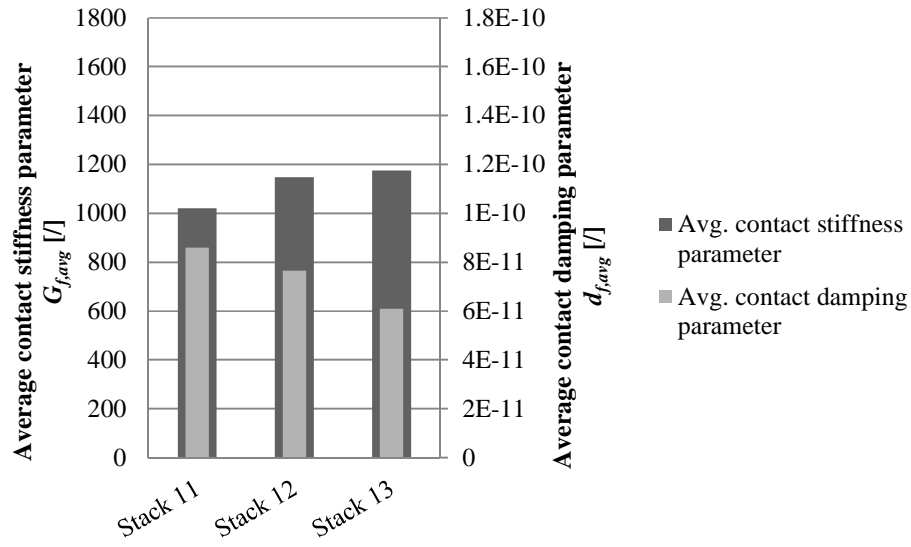


Figure 13: Effect of additional silicon layers between the steel sheets.

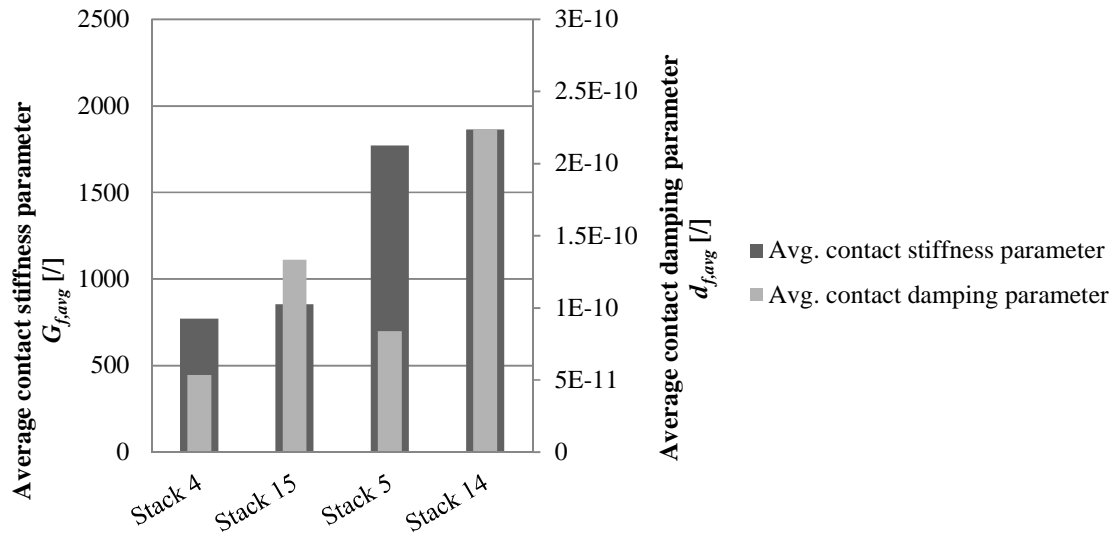


Figure 14: The effect of adhesive applied at the edges of the laminations on the contact parameters.

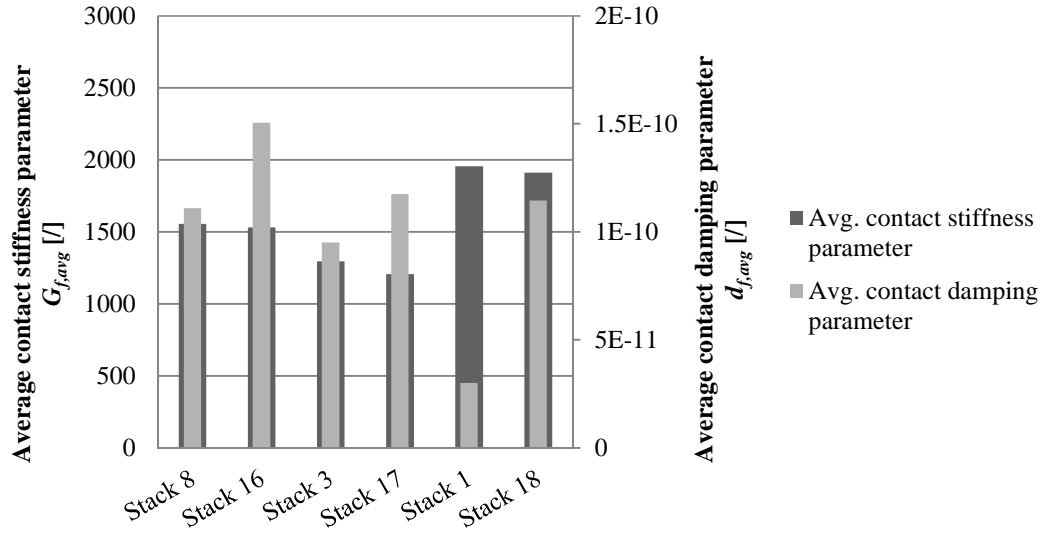


Figure 15: The effect of lubricant between the laminas on the contact parameters.

Comparison between numerically and experimentally obtained natural frequencies at a surface pressure of 320 kPa is shown in Table 7, where the error  $\varepsilon$  is defined by Eq.(2). In Fig. 16 the error  $\varepsilon$  between the experimentally and numerically obtained natural frequencies for both surface pressures is presented.

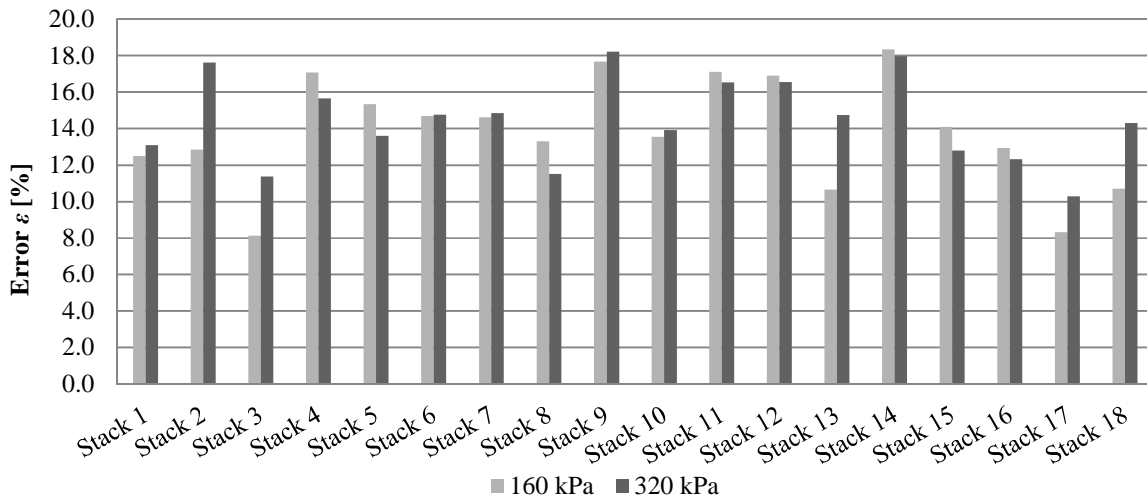
$$\varepsilon = \frac{\sum_{i=1}^4 \frac{|f_{exp,i} - f_{num,i}|}{f_{exp,i}}}{4} \cdot 100\% \quad (2)$$

Overall, the average error is approximately 14%, which can be considered as a good prediction of the numerical model when dealing with laminated structures. One has to take into consideration that the presented error is not only due to the erroneous prediction of the numerical model but is also the result of uncertainties in the experimental setup.

Table 7: Comparison between numerically and experimentally obtained natural frequencies at a surface pressure of 320 kPa.

Stack	1. Natural freq. [Hz]		2. Natural freq. [Hz]		3. Natural freq. [Hz]		4. Natural freq. [Hz]		Error $\varepsilon$ [%]
	Exp.	Num.	Exp.	Num.	Exp.	Num.	Exp.	Num.	
1	364	393.8	523	443	749	640	1017	1162.5	13.1
2	280	357	474	397	665	572	979	1104	17.6
3	289	310	408	336.5	558	484	948	1019	11.4
4	231	312	371	347	499	496	855	1030	15.7
5	335	340	487	375	701	539	1007	1075	13.6
6	238	308	372	334	511	479	896	1014	14.8
7	295	324	440	354	607	509	918	1045	14.8
8	324	348.5	450	385	626	555	966	1089	11.5
9	217	306	343	330	458	474	808	1006	18.2

10	307	329	445	370.7	645	531.2	929	1061	13.9
11	283	306.6	413	331	580	476	840	1008.1	16.5
12	284	306.7	420	331	582	476	850	1010	16.6
13	246	306	386	331	590	476	1000	1010	14.7
14	285	382	498	428.2	719	617.8	1043	1144.8	18.0
15	284	311.6	366	346.6	516	496.5	776	1027.5	12.8
16	312	356	437	392	650	565	983	1099	12.3
17	291	334.6	404	367.6	591	529.4	996	1063.1	10.3
18	328	370	467	413.4	684	535.7	1012	1125.4	14.3



**Figure 16: Average relative error between experimentally and numerically identified natural frequencies for both surface pressures.**

The presented optimization algorithm makes it possible to identify the contact parameters for various stack configurations based on a simple cube. These identified contact parameters together with the numerical model allow a calculation of the modal parameters and the dynamic response for general laminated structures.

## 4. Conclusions

A numerical model of a laminated stack applicable to general laminated structure was developed. A simple linear contact model facilitated the computational efficiency and in this way enabled the modelling of a stack with a large number of laminas. The model employs contact elements characterized by the stiffness and damping parameters in a tangential contact direction and nonlinear contact stiffness in a normal contact direction. Using the proposed linear contact model a computationally efficient numerical model was established, which made it possible to use implicit methods in the framework of the linear structural dynamics.

In order to identify the contact parameters and to validate the developed numerical model of the laminated stack several stack configurations were experimentally analysed. The experimentally identified modal parameters were then used in an optimization process to extract the contact parameters. This made

it possible to analyse the effect of the steel type, producer type, additional silicon layers and various treatments on the value of the contact parameters.

It has been shown that the friction between adjacent laminas dissipates more energy than the inserted silicon layers. An efficient way of increasing the internal damping also proved to be the application of an adhesive at the lamina edges. Furthermore, even the presence of the lubricant increased the value of damping contact parameter by as much as 150%. The average relative error between the experimentally and numerically obtained natural frequencies was approximately 14%, which can be considered as a good prediction of the numerical model when dealing with laminated structures.

## 5. References

- [1] S.D. Garvey, The vibrational behaviour of laminated components in electrical machines, *Fourth International Conference on Electrical Machines and Drives* (1989) 226-231.
- [2] J.H. Walker, G.J. Rogers, R.L. Jackson, Pressing and clamping laminated cores, *Proceedings of the Institution of electrical engineers* 111 (1964) 565-577.
- [3] K. Popp, L. Panning, W. Sextro, Vibration damping by friction forces: Theory and applications, *Journal of Vibration and Control* 9 (2003) 419-448.
- [4] W. Chen, X. Deng, Structural damping caused by micro-slip along frictional interfaces, *International Journal of Mechanical Sciences* 47 (2005) 1191-1211.
- [5] H. Bournine, D.J. Wagg, S.A. Neild, Vibration damping in bolted friction beam-columns, *Journal of Sound and Vibration* 330 (2011) 1665-1679.
- [6] A.J. Moses, S.M. Pegler, Effects of flexible bonding of laminations in a transformer core, *Journal of sound and vibration* 29 (1973) 103-112.
- [7] F. Ishibashi, S. Noda, M. Mochizuki, Numerical simulation of electromagnetic vibration of small induction motors, *IEE proceedings - electric power applications* 145 (1998) 528-534.
- [8] G.H. Jang, D.K. Lieu, The effect of magnet geometry on electric motor vibration, *IEEE Transactions on Magnetics* 27 (1991) 5202-5204.
- [9] H. Wang, K. Williams, Effects of laminations on the vibrational behaviour of electrical machine stators, *Journal of Sound and Vibration* 202 (1997) 703-715.
- [10] C. Wang, J. C. S. Lai, A. Astfalck, Sound power radiated from an inverter driven induction motor II: Numerical analysis, *IEE proceedings - electric power applications* 151 (2004) 341-348.
- [11] Z. Tang, P. Pillay, A.M. Omekanda, L. Chen, C. Cetinkaya, Young's modulus for laminated machine structures with particular reference to switched reluctance motor vibrations, *IEEE Transactions on Industry Applications* 40 (2004) 748-754.
- [12] C. Wang, J.C.S. Lai, Vibration analysis of an induction motor, *Journal of sound and vibration* 224 (1999) 733-756.
- [13] D. Torregrossa, F. Peyraut, B. Fahimi, J. M'Boua, A. Miraoui. Multiphysics Finite-Element Modeling for Vibration and Acoustic Analysis of Permanent Magnet Synchronous Machine, *IEEE Transactions on energy conservation* 26 (2011) 490-500.
- [14] M. Furlan, A. Černigoj, A coupled electromagnetic-mechanical acoustic model of a DC electric motor. *COMPEL: The International Journal for Computation and Mathematics in Electrical and Electronic Engineering* 22 (2003) 1155-1165.
- [15] G. Čepon, M. Boltežar, Dynamics of a belt-drive system using a linear complementary problem for the belt-pulley contact description, *Journal of sound and vibration* 319 (2009) 1019-1035.